Exploring Chromophore−Protein Interactions in Fluorescent Protein cmFP512 from *Cerianthus membranaceus*: X-ray Structure Analysis and Optical Spectroscopy[†]

Karin Nienhaus,[‡,§] Fabiana Renzi,[§,||] Beatrice Vallone,[||] Jörg Wiedenmann,[⊥] and G. Ulrich Nienhaus*[,‡,#]

Department of Biophysics, University of Ulm, 89069 Ulm, Germany, Department of Biochemical Sciences, University of Rome "La Sapienza", 00185 Rome, Italy, Department of General Zoology and Endocrinology, University of Ulm, 89069 Ulm, Germany, and Department of Physics, University of Illinois at Urbana−Champaign, Urbana, Illinois 61801

Received May 4, 2006; Revised Manuscript Received August 31, 2006

ABSTRACT: Autofluorescent proteins of the GFP family all share the same three-dimensional β-can fold; yet they exhibit widely different optical properties, arising either from chemical modification of the chromophore itself or from specific interactions of the chromophore with the surrounding protein moiety. Here we present a structural and spectroscopic characterization of the green fluorescent protein cmFP512 from *Cerianthus membranaceus*, a nonbioluminescent, azooxanthellate cnidarian, which has only ∼22% sequence identity with *Aequorea victoria* GFP. The X-ray structure, obtained by molecular replacement at a resolution of 1. 35 Å, shows the chromophore, formed from the tripeptide Gln-Tyr-Gly, in a hydrogen-bonded cage in the center of an 11-stranded β-barrel, tightly restrained by adjacent residues and structural water molecules. It exists in a neutral (A) and an anionic (B) species, with absorption/emission maxima at 392/460 (pH 5) and 503/512 nm (pH 7). Their fractional populations and peak positions depend sensitively on pH, reflecting protonation of groups adjacent to the chromophore. The pH dependence of the spectra is explained by a protonation mechanism involving a hydrogen-bonded cluster of charged/polar groups. Cryospectroscopy at 12 K was also performed to analyze the vibronic coupling of the electronic transitions.

The discovery of an entire family of fluorescent proteins (FPs[1]) and nonfluorescent chromoproteins (CPs) in anthozoa, hydrozoa, and copepoda that are closely related to the green fluorescent protein from *Aequorea victoria* (avGFP) has opened up a wide array of fluorescent marker proteins for cell biology (*1*−*3*). They not only present alternatives for avGFP as genetically encoded probes for the *in vivo* labeling of proteins, subcellular compartments, cells, or tissues but also feature entirely new properties, for example, red-shifted fluorescence (*4*−*8*) and photoactivatable green-to-red emission conversion (*9*−*14*). To date, more than 100 of these colorful proteins have been cloned, with emission wavelengths ranging from cyan to dark red (*1*−*8*, *10*−*32*).

The polypeptide chain of all GFP-like proteins hitherto known possesses the characteristic β-can fold, i.e., an 11-stranded β-barrel that wraps around a distorted central α-helix (*33*, *34*). Remarkably, the polypeptide chain acts as a nanoreactor in which covalent chemistry takes place: an aromatic chromophore, 4-(*p*-hydroxybenzylidene)-5-imidazolinone, is synthesized autocatalytically from three consecutive amino acids, the first of which is variable, but the second and third are always Tyr and Gly. In addition, there are two other conserved residues, Arg96 and Glu222 (in the avGFP sequence notation), which have been suggested to play key roles in chromophore formation (*35*, *36*). These observations point at a general mechanism for chromophore formation in GFP-like proteins, which involves backbone cyclization between the C′ and N backbone atoms of the first and third amino acids of the chromogenic triad, thereby creating a five-membered heterocycle; subsequent oxidation and dehydrogenation conjugates the imidazolin-5-one and Tyr hydroxyphenyl rings in a planar, delocalized π-system that fluoresces in the green spectral range (*37*−*41*). In some FPs, the delocalized π-electron system is further extended by additional covalent modifications, which result in pronounced red-shifts of the peak emission wavelength. Such modifications can occur in different ways, by an additional cyclization involving a Lys side chain, as observed in the *Zoanthus* yellow fluorescent protein zFP538 (*42*), by an additional dehydrogenation of the backbone N−Cα of the first amino acid in the triad, creating an acylimine as in the red FPs DsRed (*6*, *43*, *44*) and eqFP611 (*5*, *25*, *26*), or by formation of an *all-trans*-alkenylene structure connecting an imidazole side chain to the system, as in the green-to-red photoconverting proteins EosFP (*12*−*14*, *45*) and Kaede (*10*, *11*). While the former two modifications occur spontaneously, the latter one requires photoactivation by ∼400 nm light. In addition to these pronounced changes in the emission

[†] This work was financed by the Deutsche Forschungsgemeinschaft (SFB 569 to G.U.N.), the Fonds der Chemischen Industrie (to G.U.N.), and the Landesstiftung Baden-Württemberg (Elite-Postdoc-Förderung to J.W.).

* To whom correspondence should be addressed. E-mail: uli@uiuc.edu. Tel: +49 731 502 3050. Fax: +49 731 502 3059.

[‡] Department of Biophysics, University of Ulm.

[§] These authors contributed equally.

[||] University of Rome "La Sapienza".

[⊥] Department of General Zoology and Endocrinology, University of Ulm.

[#] University of Illinois at Urbana−Champaign.

[1] Abbreviations: GFP, green fluorescent protein; FP, fluorescent protein; ESPT, excited-state proton transfer.

10.1021/bi060885c CCC: $33.50
Published on Web 10/10/2006

wavelength due to covalent modification, smaller shifts arise from interactions of the chromophore with the surrounding protein moiety to which it is strongly coupled.

FPs have proven to be powerful tools for the life sciences. Still, further optimization by protein engineering is highly desirable to fully exploit the potential of FPs as fluorescent markers and to broaden the range of possible applications. Photophysical properties that demand optimization include photostability, brightness, and the reduction of photodynamics (blinking). To this end, we require a detailed understanding of the interplay between the protein moiety and the chromophore during and after its formation. Currently, studies of structure−dynamics−function relationships of a broad range of GFP-like proteins promise to yield new insights into the intricate interplay between the chromophore and protein matrix, which may eventually enable us to rationally engineer FPs with optimized properties for particular applications.

Here, we present a biophysical characterization of the green FP cmFP512, which was cloned from tentacle tissue of *Cerianthus membranaceus*, a nonbioluminescent, azooxanthellate cnidarian (*46*). It differs markedly from other FPs in its primary sequence, which yields only 22%, 30%, 34%, and 35% amino acid identities with avGFP, asFP499 (*47*), eqFP611 (*25*, *26*), and DsRed (*6*), respectively. The chromophore of cmFP512 is formed from the tripeptide Gln-Tyr-Gly, as is the case for DsRed. In the latter protein, however, the green chromophore is further processed to yield a red chromophore. We have performed room-temperature fluorescence and absorption spectroscopy of cmFP512 as a function of pH to explore the coupling between the chromophore and its environment. In addition, measurements were also carried out at 12 K to investigate vibronic coupling of the electronic transition. X-ray structure analysis of cmFP512, performed at a very high resolution (1. 35 Å), enables us to discuss the intriguing spectroscopic properties of cmFP512 on the basis of its molecular structure.

MATERIALS AND METHODS

Protein Expression, Purification, and Crystallization. The protein was expressed in *Escherichia coli* (strain BL21/DE3) and purified using a TALON metal affinity resin (BD Biosciences, Clontech, San Jose, CA). cmFP512 crystals were grown at 20 °C in 30% PEG 4000, 0.1 M Tris, pH 8. 5, 0.2 M magnesium chloride by using the hanging drop vapor diffusion technique, transferred to cryosolvent (26% glycerol, 30% PEG 4000, 0.1 M Tris, pH 8.5, 0.2 M magnesium chloride) and flash-frozen in liquid nitrogen immediately thereafter.

Structure Determination. Three X-ray diffraction data sets were collected from two cmFP512 crystals at 100 K at the ELETTRA synchrotron using a marCCD detector, a low-resolution data set from a first crystal (denoted by A) at 3.2 Å, and both a low (B, 1.8 Å) and a high (C, 1.35 Å) resolution data set from a second crystal. High-resolution diffraction was achieved only by using the dehydration−annealing technique. The crystals belonged to space group *P*1, with unit cell parameters $a = 54.00$ Å, $b = 60.11$ Å, $c = 125.40$ Å, $\alpha = 83.80°$, $\beta = 89.98°$, and $\gamma = 73.85°$. Reflections were indexed, reduced, and scaled with the HKL package (*48*). The structure of cmFP512 was determined by molecular replacement using MolRep (*48*), taking the structure of DsRed from *Discosoma striata* as a search model (*6*). The asymmetric unit was found to contain two tetramers related by a noncrystallographic symmetry. Model building was done manually with QUANTA (*49*) and COOT (*50*). Multiple rounds of manual rebuilding and refinement were performed. 5% of the total reflections were flagged for R_{free} cross-validation data refinement. The chromophore was built in both the $2F_o - F_c$ (contoured to 1.0 and 1.5 σ) and the $F_o - F_c$ (contoured to 3.0 σ) electron density maps. Residues 1−3 and 224−226 were not positioned; residues 4−6 (5−6) were built in 4 (6) of the eight monomers. Electron densities of the sulfur atom and the terminal methyl group Cγ of Met59 were not clearly definable. Water molecules were positioned in the electron density with COOT (*50*). Crystal parameters and data collection and refinement statistics are summarized in Table 1. Also included in the table is a Ramachandran analysis of the final model using PROCHECK (*48*), revealing excellent stereochemistry. Buried areas were calculated by AreaIMol (*48*). Graphics were produced with PyMol (*51*) and VMD (*52*). The atomic coordinates and structure factors have been deposited in the Protein Data Bank (PDB ID code 2C9J).

Table 1: Summary of Crystallographic Analysis of cmFP512[a]

Crystal Parameters and Data Collection Statistics	
temperature (K)	100
space group	*P*1
cell dimensions (Å, deg)	a = 54.00; *b* = 60.11; *c* = 125.40 α = 83.80; *b* = 89.98; γ = 73.85
unit cell volume (Å^3)	385 739.59
solvent content (%)	30.7
resolution (Å)	1.35
total no. of observations	159 486 (A); 1 474 732 (B); 330 026 (C)
no. of unique observations	300 980
mosaicity	1.4 (A); 0.5 (B); 0.5 (C)
multiplicity	1.4
data completeness (%)	90.9 (80.4)
I/σ	10.4
R_{merge}[b]	0.37 (0.63) (A); 0.05 (0.24) (B); 0.06 (0.22) (C)
Data Refinement Statistics	
non-hydrogen atoms	
protein	13 783
chromophore	192
water	2453
resolution (Å)	1.35
R_{factor}[c]	0.20
R_{free}	0.24
rms deviations from ideality	
bond lengths (Å)	0.13
bond angles (deg)	2.67
Ramachandran plot	
most favored (%)	92.5
allowed region (%)	6.2
generously allowed region (%)	1.0
disallowed (%)	0.4
B-factors (Å^2)	
overall	20
average main chain	19
average side chain	21
average chromophore	19

[a] The values in parentheses are for the highest resolution bin (approximate interval 0.15 Å). A, B, C refer to the three data sets that are scaled together with resolutions of 3.2, 1. 8 and 1.35 Å. [b] $R_{merge} = \sum((I_{hkl} - \langle I_{hkl}\rangle)^2)/\sum(I_{hkl}^2)$. [c] $R_{factor} = \sum_{hkl}||F_o| - |F_c||/\sum_{hkl}|F_o|$ for all data except for 5%, which was used for free *R* calculation.

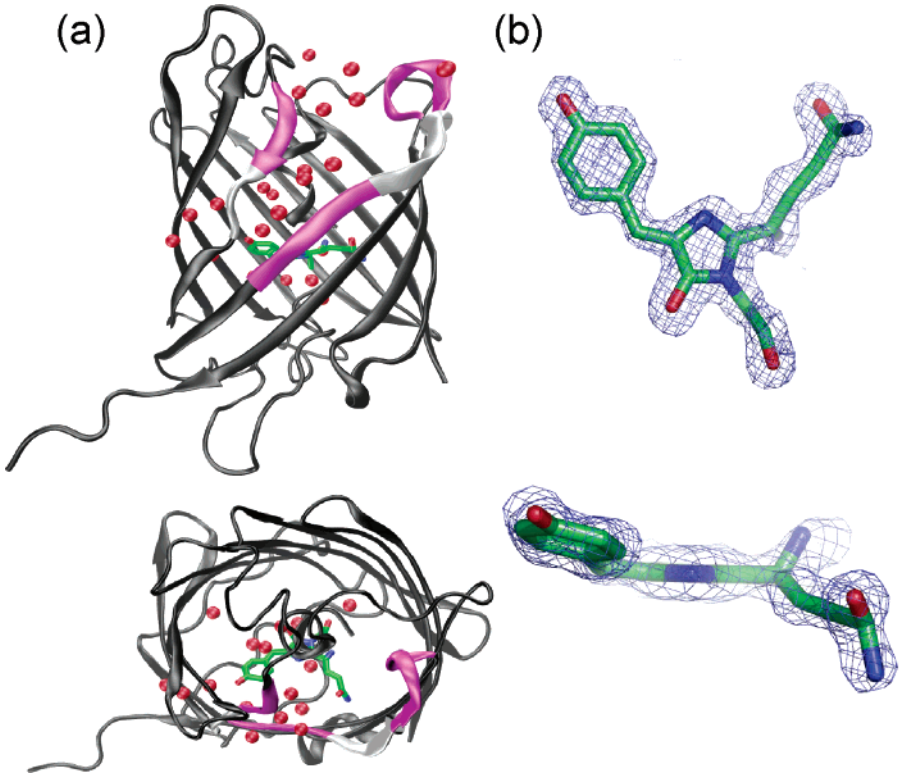

FIGURE 1: Overall fold and chromophore structure of cmFP512. (a) Cartoon representation of a cmFP512 monomer, with amino acids 137−139 (140−141) and 195−208 and 202−206 (199−201) displayed in magenta (gray). Red spheres represent water molecules. (b) $2F_o - F_c$ electron density maps of the cmFP512 chromophore contoured at 1.5 σ.

Optical Spectroscopy. Room-temperature absorption spectra were recorded on a Cary 1 spectrophotometer (Varian, Darmstadt, Germany) with a resolution of 1 nm. Low-temperature absorption spectra were collected on an OLIS-modified Cary 14 spectrometer (On-Line Instrument Systems, Bogart, GA) at a resolution of 0.4 nm. Fluorescence excitation and emission spectra were measured on a SPEX Fluorolog II spectrofluorometer (Spex Industries, Edison, NJ) with the excitation line width set to 0.85 nm. Emission spectra were recorded with 2.2 nm resolution and corrected for the wavelength dependence of the detector efficiency.

For data collection at ambient temperature, a few microliters of a concentrated cmFP512 stock solution was added to 100 mM buffer (pH < 4.5, sodium phosphate/citrate; pH 5−8.5, sodium phosphate; pH > 8.5, sodium carbonate) to obtain a final concentration of ~10 μM (absorption) and 1 μM (fluorescence), respectively. For cryospectroscopy, the stock solution was diluted in 75%/25% (vol/vol) glycerol/potassium phosphate/citrate buffer, pH 4.6 to obtain a pH 5 sample. The sample was sealed in a cuvette and attached to the cold finger of a closed-cycle helium cryostat (model 22, CTI Cryogenics, Mansfield, MA) equipped with a Lakeshore Cryotronics (Westerville, OH) model 330 digital temperature controller.

EXPERIMENTAL RESULTS AND DISCUSSION

Protein Structure

Overall Structure. In their native states, all anthozoan FPs known to date are arranged in a tetrameric quaternary structure, consisting of dimers of dimers. Despite the low sequence identity between cmFP512 and avGFP, their overall folds are essentially identical, featuring a slightly irregular, 11-stranded β-barrel (Figure 1a) (*34*). The central helix is interrupted by the chromophore which forms from the tripeptide Gln62-Tyr63-Gly64 (Figure 1b). With respect to avGFP, the average root-mean-square deviation (rmsd) of the Cα atoms is 1.32 Å; the largest structural variations are observed for amino acids 137−140 and the loop region containing amino acids 195−206 (Figure 1a). In this region, the symmetric barrel structure is markedly distorted. A cleft appears in the barrel surface that allows access of several water molecules. A close look at the structural model shows that residues Glu139-Glu140-Pro141-Ala142 on β-strand 7 form a bulge. It appears to accommodate the moiety surrounding the hydroxyphenyl oxygen of the chromophore, as is also observed in EosFP (*13*) and DsRed (*6*). This structural feature is even more obvious in avGFP, where it presumably creates the space for the two bulky side chains of Tyr145 and His148 (*33*, *34*). In cmFP512, an even more pronounced bulge, shaped from amino acids 198−201, dislodges strand 10 from the neighboring strand 7. This feature is also present in DsRed (*6*) and EosFP (*13*). The subsequent loop comprising residues 201−206 is shorter in cmFP512 than in avGFP, where it extends away from the body of the protein.

The Tetrameric Interfaces. The tetrameric subunit arrangement is held together by two types of interfaces, denoted as antiparallel and perpendicular according to the relative orientations of the symmetry axes of the cylindrical subunits. The monomers in each tetramer have an average rmsd value of their Cα atoms of 0.27 Å. The interfaces between the antiparallel cans A/B and C/D extend over two-thirds of the long axis and contain both hydrophobic and hydrophilic contacts (Table 2). Hydrophobic contacts exist between the aliphatic pair Leu121-Leu121 and the stacked pair Trp119-

Table 2: Interface Contacts and Total Buried Areas of cmFP512

	hydrophobic		hydrophilic	
A/B (antiparallel)	A	B	A	B
	Leu121 Trp119	Leu121 Trp119	Glu22 Trp119 Asn102 Asn90 Asn128	Lys15 Glu22 Asn102 Asn124 Asn20 Asn150
total buried area[a]	5771 Å^2 (33.0% of the total dimer area)			
	hydrophobic		hydrophilic	
A/C (perpendicular)	A	B	A	B
	Phe189 Phe191 Tyr170 Pro158	Pro141 Val154 Phe156 Pro158	Glu96 Gln220	Lys149 Lys193
total buried area	4266 Å^2 (33.1% of the total dimer area)			

[a] The total dimer surface area is defined as the sum of the surface areas of the monomers. The buried area is the interaction surface between the monomers, calculated with the program AreaIMol as implemented in the CCP4 suite (*48*).

Trp119; Trp119 is also hydrogen-bonded to Glu22 of the facing monomer. An electrostatic interaction involves residues Glu22 of one chain and Lys15 of the opposing chain, although Asp117 (on the same chain as Lys15) may render this interaction less efficient. Seven further hydrogen bonds provide additional stabilization of the interface, the pair Asn102-Asn102, Asn90 of one chain interacting with both Asn124 and Asn20 of the other chain, and Asn128 of one chain interacting with Asn150 of the other chain.

The perpendicular interfaces A/C and B/D are also stabilized by hydrophobic and hydrophilic interactions (Table 2); the pair Phe189-Phe191 of one monomer packs against Pro141 of the second monomer, although the backbone carbonyl of Pro141 may be detrimental for an efficient interaction. Val154 and Phe156 of one monomer create a small hydrophobic patch facing Tyr170 on the opposite monomer. The two Pro158 residues face each other in the center of the interface and induce the proximity of Phe156 to Tyr170. A salt bridge is formed between Glu96 and Lys149 of opposite monomers. The C-terminal tail of one chain grasps around the opposing monomer, resulting in the formation of another salt bridge between Lys193 and Asp220 on the C-terminus.

The Chromophore and Its Environment. The chromophore of cmFP512, 4-(*p*-hydroxybenzylidene)-5-imidazolinone (Figure 1b), is rigidly held in place by multiple hydrogen bonds to charged or polar amino acids and structural water molecules in the surroundings of the chromophore. Figure 2a displays the chromophore and its environment; hydrogen-bonding contacts are also indicated. To our surprise, our X-ray structure of cmFP512 clearly reveals that the chromophore is significantly bent, with an angle of ∼20° between the normals on the imidazolinone and phenyl rings (Figure 1b). The dihedral angles that describe the rotation of the two ring systems around the double and single bonds of the connecting bridge are $\tau = 13.25°$ and $\varphi = -14.51°$, respectively. These values are similar to the ones reported for GFP mutant S65T at pH 8 (pdb code 1EMA, $\tau = 17.6°$, $\varphi = -13°$) (*33*). Most GFP-like proteins, however, have dihedral angles around 0° (*53*).

The Gly64 backbone carbonyl is seen to interact with the Nϵ of Trp89 and two water molecules, and the carbonyl oxygen of the imidazolinone ring is hydrogen-bonded to the guanidino moiety of Arg91. The hydroxyl group of Tyr63 is engaged in two hydrogen bonds, one with a water molecule and the other with the amino group of Lys159. The water molecule is stabilized by additional interactions with the Glu140 backbone carbonyl and the Leu196 backbone N−H group (Figure 2c). The Lys159 side chain nitrogen is within hydrogen-bonding distance (2.7 Å) to one of the Glu139 side chain carboxyl oxygens. Both Glu139 carboxylic oxygen atoms are starting points of "water chains" (Figure 2a). We also note that the Gln62 side chain is held in place by hydrogen bonds of its nitrogen to the Phe38 backbone carbonyl (2.7 Å) and its oxygen to the Gln210 side chain nitrogen (2.7 Å).

Residues His194, Glu144, Arg66, and Glu212 constitute a network of polar interactions below the chromophore plane (Figure 2b). The carboxyl group of Glu144 interacts with Nϵ of His194. The Nδ atom of the latter is in hydrogen-bonding distance to an oxygen atom of the Glu212 carboxyl side chain, which again forms hydrogen bonds with both its oxygens to nitrogens on the Arg66 guanidino group. The Arg66 and Glu144 side chains are bridged by a water molecule that is also hydrogen-bonded to Tyr177. Similar networks of four hydrophilic amino acids have also been found also in other FPs, including EosFP (*13*), DsRed (*6*), amFP486 (*20*), and zFP538 (*42*).

Spectroscopic Properties

Overview. The optical absorption, excitation, and emission spectra of cmFP512 at pH 5 and 9.5, taken at ambient temperature, are presented in Figure 3; the peak wavelengths are given in Table 3. Spectra at pH 7 are indistinguishable within the experimental error from those at pH 9.5. The excitation spectra were recorded with monitoring the emission at 560 nm; the emission spectra were collected with the excitation wavelength set to 480 nm. To display the different spectra within the same plot and to compare their relative intensities, the absorption spectra were normalized at 280 nm and the excitation spectra were scaled to the absorption spectra to equal peak heights of the band at ∼500 nm. The emission spectra were scaled so as to maintain the relative fluorescence intensities at different pH.

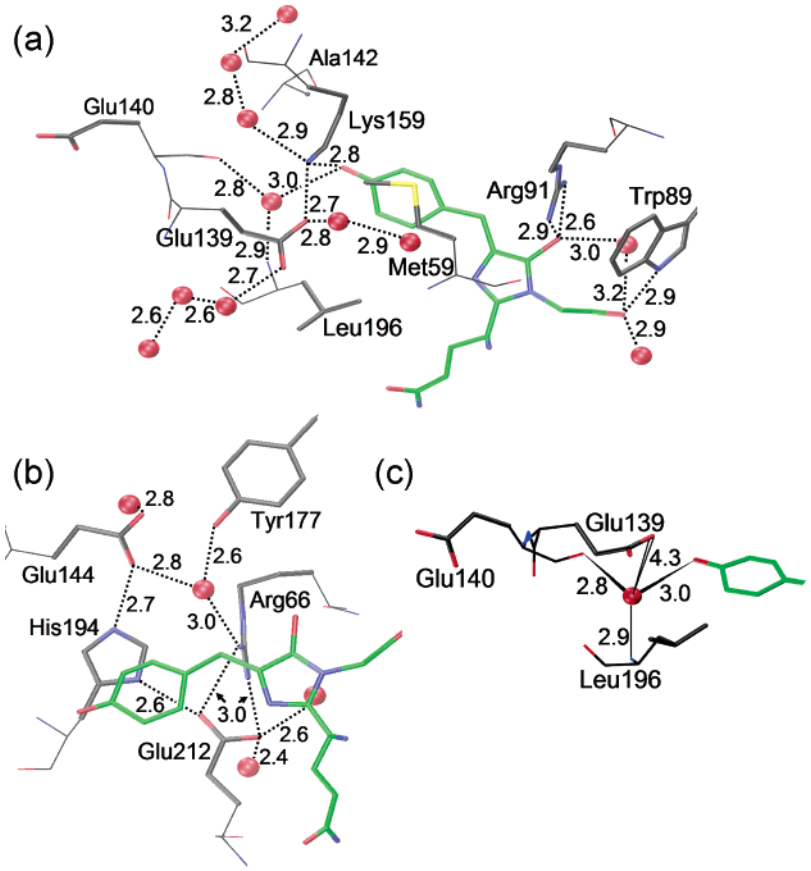

FIGURE 2: Chromophore−protein interactions in cmFP512. The chromophore and its environment are shown (a) above and (b) below the chromophore plane. (c) Tetrameric coordination of the water molecule (Wat377 in monomer A) hydrogen-bonded to the chromophore tyrosine. Chromophore color coding: green = carbon; red = oxygen; blue = nitrogen. Color coding for surrounding residues: black = carbon; red = oxygen; blue = nitrogen). The backbone structures are plotted as thin lines; the side chains are accentuated. Water molecules are represented by red spheres, hydrogen bonds by dashed lines. Distances are given in Å.

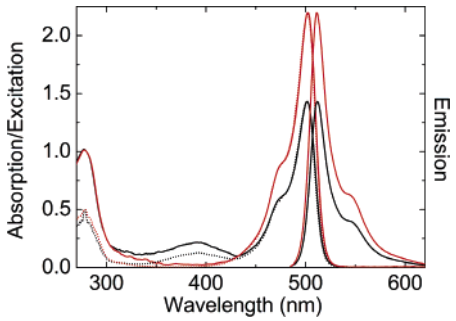

FIGURE 3: Room-temperature absorption and fluorescence spectra of cmFP512 at pH 5 (red) and 9.5 (black). Absorption spectra (bold solid lines) were scaled to unity at 280 nm. Excitation spectra (λ_{em} = 560 nm, dotted lines) were scaled to the absorption spectra to match the peak intensity of the band at ~500 nm. Emission spectra (λ_{exc} = 480 nm, solid lines) were scaled so as to maintain the relative fluorescence intensities at different pH.

The UV absorption band at 280 nm is due to aromatic side chain resonances. From the number of tyrosine (12 Tyr) and tryptophan (2 Trp) residues, we have determined the extinction coefficient at 280 nm as 29 000 M^{-1} cm^{-1}, according to the procedure reported by Pace et al. (*54*). This method yields the extinction coefficient with an accuracy of about ±5%. In the visible range, the absorption spectra exhibit a band at ~500 nm at pH 5 and 9.5, with a pronounced shoulder on the blue side, and a second band at ~390 nm only at pH 5; they are referred to as B and A bands, respectively. The presence of an A band only at low pH is typical of most anthozoan FPs. Apparently, the A and B bands correspond to different protonation states of the chromophore; they have been assigned to the neutral (phenol) and anionic (phenolate) forms of the chromophore, respectively (*28*, *55*, *56*). However, a few FPs display significant A and B species at a fairly fixed ratio over a wide pH range; among these are wild-type avGFP (*55*, *57*) and asFP499 from *Anemonia sulcata* (*31*, *47*).

The excitation spectra at pH 9.5 track the absorption spectrum between 330 and 550 nm. At 280 nm, however, the excitation peak is markedly smaller than the absorption peak, indicating that the efficiency of Förster transfer from aromatic residues to the chromophore is less than 50%. At pH 5, the excitation spectrum matches the absorption spectrum only in the B band, but deviates in both the A and 280 nm bands. The occurrence of emission at 560 nm upon excitation in the A band arises from a mechanism denoted as excited-state proton transfer (ESPT), which is well-known from photophysical studies of avGFP (*56*, *58*): Excitation of the neutral species yields the A* state that undergoes excited-state deprotonation on the picosecond time scale to form the anionic, intermediate I* form emitting at 504 nm, which subsequently relaxes to the anionic B* species emitting at 508 nm. In avGFP, both theory (*59*) and experiment (*60*) have implicated Glu222 as the proton acceptor in ESPT. In cmFP512, the corresponding residue Glu212 is part of a network of charged residues and, therefore, not likely to be involved in ESPT (Figure 2b). The fact that the A band is

Table 3

	λ_{max} (pH 5/pH 9.5) (nm)[a]	ν_{0-0}[b] cm^{-1} (nm)	ν_1[b] cm^{-1} (nm)	ν_2[b] cm^{-1} (nm)	ν_3[b] cm^{-1} (nm)
cmFP512					
excitation A	392/−	23450 (426.5)	350 (420.2)	1700 (397.6)	
excitation B	502.2/502.6	19800 (505.1)	85 (502.9)	880 (483.6)	1410 (471.5)
emission A	(∼460)/−		340 (432.7)	1830 (462.5)	
emission B	511.9/512.4		85 (507.2)	900 (528.5)	1470 (545.4)
avGFP[c]					
excitation A		23041 (434)	270	880	1710
excitation B		20964 (477)	222	775	1507
excitation I		20202 (495)	248		
emission A				570	1440
emission B			220	765	1509
emission I			242	934	1683

[a] Data taken at room temperature (290 K). [b] These data were collected on a pH 5 sample at 12 K. Values in parentheses are peak positions given in nm. Peak positions have been determined with an error of ±0.5 nm, which corresponds to ±30 cm^{-1} for the transition frequencies. [c] Data on avGFP are taken from ref *76*. They were collected at 1.6 K.

less intense in the excitation spectrum than in the absorption spectrum indicates that a significant fraction of neutral chromophores fluoresces at a different wavelength or does not fluoresce at all (*vide infra*).

The emission band of the anionic species peaks at 512 nm and has a shoulder at 548 nm (Figure 3); its shape is independent of pH. Compared with avGFP, which peaks at 508 nm, the emission of cmFP512 is shifted to the red. We note that the mutant Ala142Ser of cmFP512 has its emission peak at 507 nm (data not shown). The X-ray structure of wild-type cmFP512 suggests that the hydroxyl group of a Ser in the place of Ala142 is in hydrogen-bonding distance to the chromophore hydroxyl, with the distance between the two oxygen atoms estimated as 2.5 Å. Indeed, in a variety of X-ray structures of GFP-like proteins, including DsRed (*6*), amFP486 (*20*), asFP499 (*47*), and EosFP (*13*), the chromophore Tyr hydroxyl interacts with a Ser side chain within a distance of 2.5−2.7 Å. The additional hydrogen bond apparently stabilizes the charge on the hydroxyphenyl moiety and thus the ground state of the anionic species. The mutant contains essentially only the anionic species, which does not convert to the neutral species at lower pH, as the spectra are identical between pH 4 and 11. A similar interaction pattern at the phenolate oxygen is observed for DsRed, and likewise, its chromophore also exists solely in the anionic form (*6*). The blue shift of the emission spectrum of the Ala142Ser mutant by 5 nm implies that the excited state is less stabilized or destabilized with respect to the ground state by the additional hydrogen bond, as one would expect on electrostatic grounds from the fact that the electron density shifts from the phenol moiety toward the heterocycle in the excited state (*61*−*63*).

Fluorescence from the Neutral Chromophore. In avGFP, ESPT is very efficient, and direct A* emission is visible only as a very weak band at ∼460 nm on the wing of the main 508 nm emission (*56*, *64*−*66*). Recent time-resolved studies have shown that the A* emission band is rather wide, with weak vibronic structure (*65*). Enhanced A* emission was observed by Remington and co-workers in EGFP mutants that were designed to interrupt the ESPT pathway between chromophore and proton acceptor (*64*).

To examine the fluorescence properties of the neutral cmFP512 chromophore, excitation spectra were measured from 280 to 450 nm between pH 2.5 and 6, with the detection wavelength set to 455 nm (Figure 4a). The spectra were

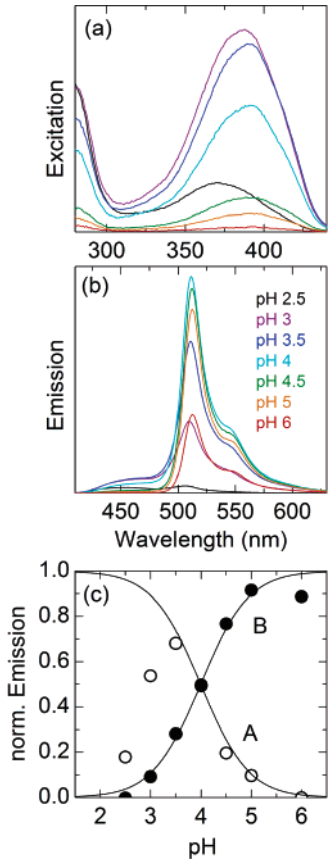

FIGURE 4: pH dependence of cmFP512 fluorescence at room temperature. (a) Excitation (λ_{em} = 455 nm) and (b) emission (λ_{exc} = 390 nm) spectra between pH 2.5 and 6. (c) pH dependence of the quantum efficiency for emission at 455 and 512 nm upon excitation in the A band at 390 nm.

normalized according to the absorption spectra so as to remove effects of varying concentrations. Between pH 3 and 6, the excitation band peaks at 390 nm and tracks the absorption after scaling, indicating that the observed changes with pH are entirely due to variations in the absorbance and not in the quantum yield of emission from A*. At pH 2.5, however, the amplitude is only about one-third of the value expected from the absorption spectrum, and the peak maximum is shifted by almost 20 to 370 nm.

We also collected emission spectra of the samples between 395 and 700 nm, with the excitation wavelength set to 390 nm. These data are shown in Figure 4b, again scaled

according to the absorption spectra to remove effects of varying protein concentration. Besides the dominant emission band from the unprotonated chromophore at 512 nm, they also show a broad emission band from the neutral chromophore peaking at ~460 nm. Its relative intensity increases with decreasing pH. At pH 3, the relative spectral area is maximal and amounts to ~25% of the total.

In Figure 4c, we present the efficiency for emission in the A (455 nm) and B (512 nm) bands, normalized to equal probability for excitation at 390 nm. These data show that the probability of B band emission increases with pH, with a dependence consistent with a Henderson−Hasselbalch relation, $(1 + 10^{(pK_a - pH)})^{-1}$, with p$K_a \approx 4$ (line). This suggests that the efficiency of ESPT depends on deprotonation of a group with p$K_a \approx 4$. Accordingly, the efficiency of A band emission deteriorates toward higher pH values, as expected for such a model. For avGFP, Glu222 has been identified as the final proton acceptor (*59*, *60*). In cmFP512, the corresponding residue Glu212 is part of a network of charged residues that is not connected to the hydroxyl of Tyr63 (Figure 2b) and, therefore, not likely to be not involved in ESPT. A possible candidate is Glu139 in the close vicinity of the Tyr63 hydroxyl. Further support is provided by the analysis of the pH dependence of the absorption spectra (*vide infra*).

Below pH 3.5, the emission probability of A* deteriorates drastically, suggesting that the protein denatures and, as a consequence, the chromophore is no longer shielded from the solvent and its fluorescence is quenched (*67*, *68*). This interpretation is also supported by the shift of the A band excitation peak to ~370 nm, which is similar to the absorption peak of the neutral model chromophore HBMIA (ethyl 4′-hydroxybenzylidene-2-methyl-imidazolinone-3-acetate) in water (368 nm) (*69*, *70*). Rapid internal conversion has been identified as the mechanism of radiationless decay (*71*−*75*). Its weak viscosity dependence suggests a volume-conserving transition, and the associated reaction barrier is low. It is still a conundrum how the protein moiety is able to suppress such an efficient radiationless decay channel. Finally, we note that direct emission from A* is more pronounced at cryogenic temperatures, where it amounts to ~50% of the overall fluorescence signal in a pH 5 sample at 12 K (*vide infra*).

Absorption Spectra and Their Dependence on Proton Concentration. To investigate the pH dependence of the A and B forms of the chromophore in detail, we collected absorption spectra from pH 1−12 (Figure 5a). At the extreme values of pH, the protein is completely denatured, as inferred from the typical bands of the acid (dotted line) and base (dashed line) denatured species at 382 and 447 nm (*47*, *67*). We have calculated their peak molar extinction coefficients as 23 800 and 29 000 M^{-1} cm^{-1}, respectively, by referencing to the extinction coefficient of 29 000 M^{-1} cm^{-1} at 280 nm.

At pH 7, all chromophores are in the anionic B form, with a peak molar extinction coefficient of 58 000 M^{-1} cm^{-1}. The determination of the extinction coefficient of the neutral A species is a little bit more involved because acid denaturation sets in below pH 3.5, where we still have a measurable fraction of B chromophores. Therefore, we have measured the A band absorption at pH 4.5 and rescaled it for the fraction of chromophores still in the B band (59 ± 1%). Based on the 280 nm extinction coefficient, we have computed the peak molar extinction coefficient of the neutral species as 21 000 M^{-1} cm^{-1}.

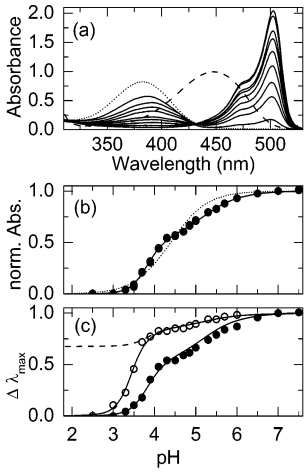

FIGURE 5: pH dependence of the cmFP512 absorption spectra between pH 1 and 12. (a) Absorption spectra of cmFP512 between pH 2 and pH 8 (solid lines). The spectra of the acid (pH 1) and base (pH 12) denatured forms are included as dotted and dashed lines, respectively. (b) Filled circles: Normalized area of the B band. Solid line: Fit with the two-site protonation model (Figure 6). Dotted line: Henderson−Hasselbalch relation with p$K_a = 4.5$. (c) Filled circles: Normalized shift of the B band. The solid line through the data is identical to the one in panel b. Open circles: Normalized line shift of the A band. The solid line is a sum of the line from panel b, also given as a dashed line, and a Henderson−Hasselbalch transition (p$K_a = 3.5$, $n = 3$).

Figure 5b displays the fractional population in the B state (circles) as a function of pH. For a simple protonation equilibrium involving only the neutral (*HY*) and the anionic (Y^-) chromophore species, we would expect a pH dependence of the relative fraction of deprotonated species according to the Henderson−Hasselbalch relation,

$$f_{Y^-}(\mathrm{pH}) = \frac{1}{1 + 10^{n(\mathrm{p}K_a - \mathrm{pH})}} \qquad (1)$$

with $n = 1$; $n > 1$ indicates a cooperative transition that involves multiple protonating groups. This one-step function, depicted in Figure 5b for p$K_a = 4.5$ and $n = 1$ as the dotted line, obviously does not describe the pH dependence of the B state population. The data rather suggest a two-step behavior, which can be modeled by a more complex scheme that involves (at least) one other protonating group, which we shall denote by *X*. This group resides in the vicinity of the protonating chromophore group *Y* so as to modulate its proton affinity via electrostatic interactions. For symmetry reasons, *Y* also influences the proton affinity of *X* so that we have to consider altogether four species, YH/XH, YH/X^-, Y^-/XH and Y^-/X^-, shown in the scheme in Figure 6. Their relative populations are governed by four equilibrium coefficients K_{a1}−K_{a4}:

$$K_{a1} = \frac{[Y^- XH][H^+]}{[YHXH]}, \qquad K_{a2} = \frac{[Y^- X^-][H^+]}{[Y^- XH]},$$
$$K_{a3} = \frac{[YHX^-][H^+]}{[YHXH]}, \qquad K_{a4} = \frac{[Y^- X^-][H^+]}{[YHX^-]} \qquad (2)$$

or, likewise, their corresponding pK_a values, with $pK_a = -\log K_a$. We also note that

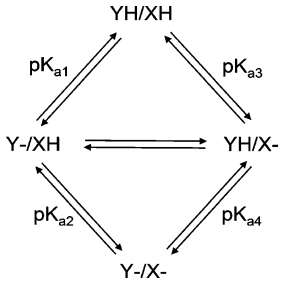

FIGURE 6: Two-site protonation model describing the pH dependence of the population of the anionic species (Figure 5b).

$$pK_{a1} + pK_{a2} = pK_{a3} + pK_{a4} \quad (3)$$

The fractional populations of the four species as a function of pH are calculated from

$$f_{YHXH}(pH) = 1/(1 + 10^{x_1} + 10^{x_3} + 10^{(x_1+x_2)})$$

$$f_{Y^-XH}(pH) = 10^{x_1}/(1 + 10^{x_1} + 10^{x_3} + 10^{(x_1+x_2)})$$

$$f_{YHX^-}(pH) = 10^{x_3}/(1 + 10^{x_1} + 10^{x_3} + 10^{(x_1+x_2)})$$

$$f_{Y^-X^-}(pH) = 10^{(x_1+x_2)}/(1 + 10^{x_1} + 10^{x_3} + 10^{(x_1+x_2)}) \quad (4)$$

with $x_i = pH - pK_{ai}$. The overall population of molecules with an anionic chromophore is then given by

$$f_{Y^-}(pH) = f_{Y^-XH}(pH) + f_{Y^-X^-}(pH) \quad (5)$$

When fitting our data with this model, we realized that the low-pH step is far too steep for a single protonation. Therefore, we included a cooperativity parameter n for the low-pH equilibria 1 and 3, so that $x_i = n(pH - pK_{ai})$ for $i = 1, 3$ (see Figure 6). The solid line in Figure 5b shows that this model provides an excellent description of the data, with fit parameters $n = 2.1 \pm 0.1$, $pK_{a1} = 4.0 \pm 0.1$, $pK_{a2} = 4.8 \pm 0.1$, $pK_{a3} = 4.0 \pm 0.1$, and $pK_{a4} = 4.8 \pm 0.1$. According to this model, the chromophore pK_a is 4.0 in the presence and 4.8 in the absence of a proton on the neighboring group X. The pK_a difference of 0.8 unit corresponds to an interaction free energy of 4.5 kJ/mol between groups X and Y. From inspection of the parameters, we realize that both protonating groups have identical pK_a values within the experimental error, which is a direct consequence of the fact that the step in the data in Figure 5b occurs at ~50% fractional protonation.

In addition to the change in the population ratio, we have noticed distinct shifts in the positions of the A and B bands in the same range of pH. These band shifts arise from a coupling of the delocalized π-electron system of the chromophore to changes in the electrostatic environment. The B band peaks at 500.8 nm at pH 3 and 2.0 nm higher at pH 9. In Figure 5c, the fractional shift (closed circles) is plotted together with the curve obtained from the fit of the fractional population in Figure 5b (solid line). It is evident that this function fits the B band shift very well. This agreement poses a serious puzzle, however: in the simple two-site protonation model in Figure 6, shifts in the anionic B band can only arise from protonation of the other group X, and consequently, the shift should only reveal a single protonation transition of X with $pK_a = 4.8$. The B band shift, however, suggests that protonation of group X changes with pH in exactly the same fashion as group Y, i.e., the chromophore itself.

For the A band, a much larger shift occurs, from 382.9 nm at pH 1 to 394.0 nm at pH 6, which is also plotted in Figure 5c normalized between 0 and 1 (open circles). Close inspection again reveals a step with $pK_a = 4.8$ and an amplitude of 1.7 nm, similar in size as for the B band. Therefore, we chose to model these data again with the pH dependence of Figure 5b (dashed line). In addition, we fitted the large-amplitude, low-pH step, with a cooperative transition, eq 1, which yielded a fractional amplitude of 0.68 ± 0.05, $pK_a = 3.4 \pm 0.1$, and $n = 3.3 \pm 0.2$. This low-pH transition reflects cooperative unfolding of the protein because the low-pH endpoint is at the position of the acid-denatured species. Note that this behavior also coincides with the observed collapse of the fluorescence emission from A* at low pH (Figure 4c). Although the denaturation transition overlaps partially with the shift at higher pH, the step with $pK_a = 4.8$ strongly suggests that the pH dependence depicted in Figure 5b is also present in the A band.

The X-ray structure provides clues as to how to reconcile the apparently contradictory findings from the fractional population of the B band on the one hand and the shifts of both A and B bands on the other. Clearly, groups in the close vicinity of the hydroxyphenyl moiety of the chromophore ought to be responsible for its protonation probability and wavelength shifts with pH (Figure 2). The Tyr63 side chain oxygen is 2.8 Å away from the Lys159 side chain Nζ, which in return resides within 2.7 Å of one of the two Glu139 carboxyl oxygens. In addition, a water molecule is situated close by (Figure 2c), forming hydrogen bonds to the Tyr63 hydroxylic oxygen, to the Leu196 backbone nitrogen, and to the Glu140 backbone carbonyl. Charges on Glu139, Lys159, Tyr63, and the water molecule will have significant electrostatic interaction energies. We suggest that these four groups form a tightly coupled hydrogen-bonded cluster that behaves as a single protonating entity (Figure 7). Above pH 7, its net charge is −1 due to the negative Glu139 and Tyr63 and the positive Lys159. As the pH is lowered, the cluster takes up a proton with $pK_a = 4.8$ and thus becomes overall neutral. In the X-ray structure at pH 8.5, the distance between the water and the Glu139 carboxyl (4.3 Å) is too long for a hydrogen bond; it rather reflects mutual repulsion of the two lone-pair orbitals. In the neutral cluster, however, this gap can be bridged by the additional proton, and Glu139 can rearrange so as to position its carboxylic oxygen in hydrogen-bonding distance to the water molecule. In the two-site model of Figure 6, the proton can reside only on either of two groups, and consequently, shifts in the B (A) band should only reflect protonation of X (i.e., Glu139) for a (de-)protonated chromophore. In the neutral state of the cluster in Figure 7, a proton can shuttle between Glu139 and the water molecule when the chromophore is in the anionic B as well as the neutral A state. Therefore, band shifts reflecting the relative fractions of protons in both positions are observable in both bands. The fact that the two-site protonation model yields identical pK_a values connecting the two neutral species with the two charged species lends further credence to the cluster model, in which there is a single neutral state comprising four rapidly interconverting protonation patterns with similar Gibbs free energies.

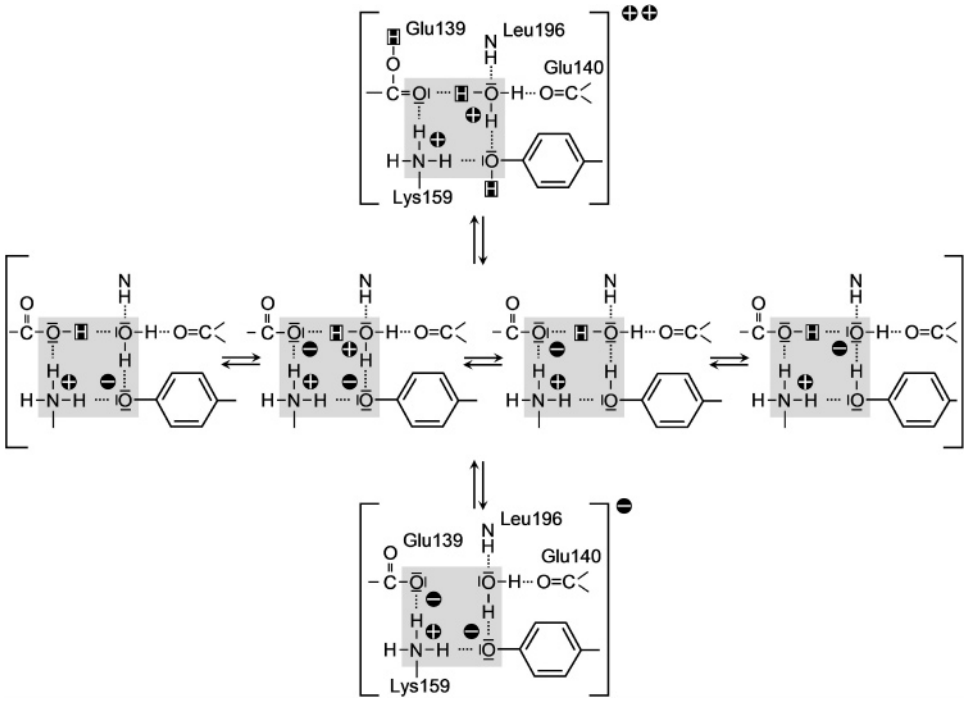

FIGURE 7: Schematic representation of the cluster of protonation sites in the vicinity of the phenolic oxygen of the chromophore. Depicted are (from top to bottom) the doubly protonated, low-pH species, the four possible neutral species, and the negatively charged, high-pH state.

The cooperativity parameter $n \approx 2$ of the second protonation step at low pH suggests that the neutral cluster picks up two more protons in a cooperative transition. Indeed, Figure 7 shows that a charge of +2 can be realized if both Glu139 and Tyr63 are neutral, Lys159 is positively charged, and a hydronium ion resides at the water position. Thus, the immediate environment of the hydroxyphenyl side chain is saturated with protons. As a consequence, excitation of the neutral chromophore leads to direct emission of A* because ESPT from the chromophore to another group in the environment is no longer feasible (Figure 4c).

Vibrational Coupling of Electronic Transitions. To study the coupling between electronic and vibrational transitions, we cooled a cmFP512 sample to 12 K, which leads to a sharpening of the lines and thus to a better resolution of vibronic side bands. In Figure 8, we compare the excitation and emission spectra of a pH 5 sample measured at 290 and 12 K. At 290 K, B band excitation peaks at 502 nm upon detection at 555 nm (Figure 8a). A small A excitation band is also seen at ~390 nm due to ESPT. Upon detection of direct A* emission at 455 nm, we observe an even smaller excitation band at ~390 nm. Excitation with 480 nm light leads to B* emission at 512 nm; it is much stronger than the one observed with 390 nm light because the latter excites the A band population only. At 12 K, the A band area is significantly larger than at room temperature, indicating that the population has shifted to the species with lower enthalpy, which is apparently the neutral chromophore species (Figure 8b). The excitation spectrum of the A band is still very broad, covering the range from 370 to 430 nm. The second derivative spectrum in Figure 8c indicates that it can be decomposed into two peaks at 420.2 and 397.6 nm and a weaker feature at ~380 nm, which appears only as a shoulder on the blue side of the spectrum. The first two peaks are also clearly seen in the emission spectrum with excitation at 390 nm, which reveals a large fraction of direct emission

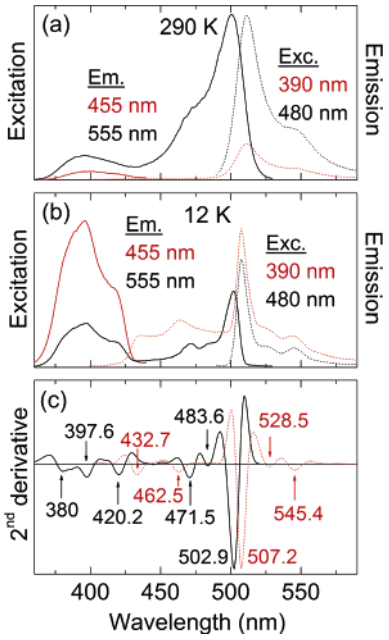

FIGURE 8: Excitation and emission spectra of a pH 5 sample of cmFP512 at 290 and 12 K. Excitation (red solid, λ_{em} = 455 nm; black solid, λ_{em} = 555 nm) and emission (red dotted, λ_{exc} = 390 nm; black dotted, λ_{exc} = 480 nm) spectra of cmFP512 (pH 5) at (a) 290 and (b) 12 K. (c) Second derivatives of the excitation (λ_{em} = 555 nm) and emission (λ_{exc} = 390 nm) spectra plotted in panel b.

from the A band at 12 K. This mirror-symmetric arrangement of the excitation and emission bands allows us to locate the 0−0 transition of the A band at 426.5 nm. The Stokes shift, i.e., the energetic separation between the first two peaks, is ~700 cm^{-1}, and the vibrations most strongly coupled to the electronic transition are at ~350 and in the range 1700−1800 cm^{-1}. For the anionic chromophore, the B excitation band peaks at 502.9 nm, slightly blue-shifted from 503.9

nm at pH 8 (data not shown). The emission maximum of the anionic species is at 507.2 nm upon excitation at 480 nm, blue-shifted by 4.4 ± 0.3 nm with respect to ambient temperature and less intense (Figure 8b). Side bands are well resolved at 528.5 and 545.4 nm (Figure 8c). The 0−0 transition of the B band is located at 505.1 nm, and the Stokes shift is only ∼170 cm^{-1}. The vibrations most strongly coupled to the electronic transition are at ∼85, ∼900, ∼1400 cm^{-1}. The 0−0 transitions and the sidebands are compiled in Table 3, together with the data on avGFP from spectral hole burning experiments at 1.6 K (*76*).

The lowest frequencies, 350 (A) and 85 (B) cm^{-1}, are likely an average over several modes and thus represent a low-frequency bath. Remarkably, protonation of the chromophore has such a strong influence on the low-frequency coupling. For avGFP, low-frequency vibrations were reported at 220 (B) and 242 (I) (*76*), and moreover, the high-frequency vibrations were also in a range similar to our findings. The latter correspond to local modes of the chromophore coupled to the electronic transition. Frequencies at 900, 1400, and 1700 cm^{-1} have been observed by vibrational spectroscopy on GFP and the model chromophore HBDI, but unambiguous assignments cannot be made at present (*69*, *77*, *78*). Only the mode at ∼1700−1800 cm^{-1} in the A form of cmFP512 most likely arises from coupling to the C═O stretching vibration of the imidazolinone (*77*, *78*).

CONCLUSIONS

The widespread interest in FPs is based on different motivations. On the one hand, there is a strong impetus to discover and/or design marker proteins with advanced or entirely novel properties to serve as fluorescent markers in cell biology applications. On the other hand, there is the basic quest for a better understanding of GFP-like proteins at the molecular level, especially the mechanism of chromophore formation and the interactions between the chromophore and the amino acid scaffold that are responsible for their peculiar photophysical properties. Here we have studied the spectroscopic properties of cmFP512 in great detail. By focusing on the intriguing pH dependence of its spectroscopic properties, interactions of the chromophore with the surrounding protein moiety could be elucidated and interpreted on the basis of the X-ray structure at very high resolution. Comparative studies of structure−function relationships in a variety of naturally occurring FPs will provide a picture of how structural variations affect the function and thus give guidance toward a rational approach of optimization of GFP-like proteins, based on a solid knowledge of the physics and chemistry of proteins.

REFERENCES

1. Chudakov, D. M., Lukyanov, S., and Lukyanov, K. A. (2005) Fluorescent proteins as a toolkit for in vivo imaging, *Trends Biotechnol. 23*, 605−613.
2. Chapman, S., Oparka, K. J., and Roberts, A. G. (2005) New tools for in vivo fluorescence tagging, *Curr. Opin. Plant Biol. 8*, 565−573.
3. Zhang, J., Campbell, R. E., Ting, A. Y., and Tsien, R. Y. (2002) Creating new fluorescent probes for cell biology, *Nat. Rev. Mol. Cell Biol. 3*, 906−918.
4. Wiedenmann, J., Schenk, A., Röcker, C., Girod, A., Spindler, K. D., and Nienhaus, G. U. (2002) A far-red fluorescent protein with fast maturation and reduced oligomerization tendency from Entacmaea quadricolor (Anthozoa, Actinaria), *Proc. Natl. Acad. Sci. U.S.A. 99*, 11646−11651.
5. Wiedenmann, J., Vallone, B., Renzi, F., Nienhaus, K., Ivanchenko, S., Röcker, C., and Nienhaus, G. U. (2005) The red fluorescent protein eqFP611 and its genetically engineered dimeric variants, *J. Biomed. Optics 10*, 014003 (7 pages).
6. Yarbrough, D., Wachter, R. M., Kallio, K., Matz, M. V., and Remington, S. J. (2001) Refined crystal structure of DsRed, a red fluorescent protein from coral, at 2.0-A resolution, *Proc. Natl. Acad. Sci. U.S.A. 98*, 462−467.
7. Baird, G. S., Zacharias, D. A., and Tsien, R. Y. (2000) Biochemistry, mutagenesis, and oligomerization of DsRed, a red fluorescent protein from coral, *Proc. Natl. Acad. Sci. U.S.A. 97*, 11984−11989.
8. Campbell, R. E., Tour, O., Palmer, A. E., Steinbach, P. A., Baird, G. S., Zacharias, D. A., and Tsien, R. Y. (2002) A monomeric red fluorescent protein, *Proc. Natl. Acad. Sci. U.S.A. 99*, 7877−7882.
9. Wiedenmann, J., and Nienhaus, G. U. (2006) Live-cell imaging with EosFP and other photoactivatable marker proteins of the GFP family, *Expert Rev. Proteomics 3*, 361−374.
10. Ando, R., Hama, H., Yamamoto-Hino, M., Mizuno, H., and Miyawaki, A. (2002) An optical marker based on the UV-induced green-to-red photoconversion of a fluorescent protein, *Proc. Natl. Acad. Sci. U.S.A. 99*, 12651−12656.
11. Mizuno, H., Mal, T. K., Tong, K. I., Ando, R., Furuta, T., Ikura, M., and Miyawaki, A. (2003) Photo-induced peptide cleavage in the green-to-red conversion of a fluorescent protein, *Mol. Cell 12*, 1051−1058.
12. Nienhaus, G. U., Nienhaus, K., Hölzle, A., Ivanchenko, S., Renzi, F., Oswald, F., Wolff, M., Schmitt, F., Röcker, C., Vallone, B., Weidemann, W., Heilker, R., Nar, H., and Wiedenmann, J. (2005) Photoconvertible Fluorescent Protein EosFP-Biophysical Properties and Cell Biology Applications, *Photochem. Photobiol. 82*, 351−358.
13. Nienhaus, K., Nienhaus, G. U., Wiedenmann, J., and Nar, H. (2005) Structural basis for photo-induced protein cleavage and green-to-red conversion of fluorescent protein EosFP, *Proc. Natl. Acad. Sci. U.S.A. 102*, 9156−9159.
14. Wiedenmann, J., Ivanchenko, S., Oswald, F., Schmitt, F., Röcker, C., Salih, A., Spindler, K. D., and Nienhaus, G. U. (2004) EosFP, a fluorescent marker protein with UV-inducible green-to-red fluorescence conversion, *Proc. Natl. Acad. Sci. U.S.A. 101*, 15905−15910.
15. Bevis, B. J., and Glick, B. S. (2002) Rapidly maturing variants of the Discosoma red fluorescent protein (DsRed), *Nat. Biotechnol. 20*, 83−87.
16. Bell, A. F., Stoner-Ma, D., Wachter, R. M., and Tonge, P. J. (2003) Light-driven decarboxylation of wild-type green fluorescent protein, *J. Am. Chem. Soc. 125*, 6919−6926.
17. Chudakov, D. M., Belousov, V. V., Zaraisky, A. G., Novoselov, V. V., Staroverov, D. B., Zorov, D. B., Lukyanov, S., and Lukyanov, K. A. (2003) Kindling fluorescent proteins for precise in vivo photolabeling, *Nat. Biotechnol. 21*, 191−194.
18. Fradkov, A. F., Chen, Y., Ding, L., Barsova, E. V., Matz, M. V., and Lukyanov, S. A. (2000) Novel fluorescent protein from Discosoma coral and its mutants possesses a unique far-red fluorescence, *FEBS Lett. 479*, 127−130.
19. Heim, R., Cubitt, A. B., and Tsien, R. Y. (1995) Improved green fluorescence, *Nature 373*, 663−664.
20. Henderson, J. N., and Remington, S. J. (2005) Crystal structures and mutational analysis of amFP486, a cyan fluorescent protein from Anemonia majano, *Proc. Natl. Acad. Sci. U.S.A. 102*, 12712−12717.
21. Karasawa, S., Araki, T., Nagai, T., Mizuno, H., and Miyawaki, A. (2004) Cyan-emitting and orange-emitting fluorescent proteins as a donor/acceptor pair for fluorescence resonance energy transfer, *Biochem. J. 381*, 307−312.
22. Karasawa, S., Araki, T., Yamamoto-Hino, M., and Miyawaki, A. (2003) A green-emitting fluorescent protein from Galaxeidae coral and its monomeric version for use in fluorescent labeling, *J. Biol. Chem. 278*, 34167−34171.
23. Miyawaki, A., Nagai, T., and Mizuno, H. (2005) Engineering fluorescent proteins, *Adv. Biochem. Eng. Biotechnol. 95*, 1−15.
24. Mizuno, H., Sawano, A., Eli, P., Hama, H., and Miyawaki, A. (2001) Red fluorescent protein from Discosoma as a fusion tag and a partner for fluorescence resonance energy transfer, *Biochemistry 40*, 2502−2510.

25. Nienhaus, K., Vallone, B., Renzi, F., Wiedenmann, J., and Nienhaus, G. U. (2003) Crystallization and preliminary X-ray diffraction analysis of the red fluorescent protein eqFP611, *Acta Crystallogr. D 59*, 1253−1255.
26. Petersen, J., Wilmann, P. G., Beddoe, T., Oakley, A. J., Devenish, R. J., Prescott, M., and Rossjohn, J. (2003) The 2.0-A crystal structure of eqFP611, a far red fluorescent protein from the sea anemone Entacmaea quadricolor, *J. Biol. Chem. 278*, 44626−44631.
27. Shagin, D. A., Barsova, E. V., Yanushevich, Y. G., Fradkov, A. F., Lukyanov, K. A., Labas, Y. A., Semenova, T. N., Ugalde, J. A., Meyers, A., Nunez, J. M., Widder, E. A., Lukyanov, S. A., and Matz, M. V. (2004) GFP-like Proteins as Ubiquitous Metazoan Superfamily: Evolution of Functional Features and Structural Complexity, *Mol. Biol. Evol. 21*, 841−850.
28. Tsien, R. Y. (1998) The green fluorescent protein, *Annu. Rev. Biochem. 67*, 509−544.
29. Wachter, R. M., King, B. A., Heim, R., Kallio, K., Tsien, R. Y., Boxer, S. G., and Remington, S. J. (1997) Crystal structure and photodynamic behavior of the blue emission variant Y66H/Y145F of green fluorescent protein, *Biochemistry 36*, 9759−9765.
30. Wachter, R. M., Elsliger, M. A., Kallio, K., Hanson, G. T., and Remington, S. J. (1998) Structural basis of spectral shifts in the yellow-emission variants of green fluorescent protein, *Structure 6*, 1267−1277.
31. Wiedenmann, J., Elke, C., Spindler, K. D., and Funke, W. (2000) Cracks in the beta -can: fluorescent proteins from Anemonia sulcata (Anthozoa, Actinaria), *Proc. Natl. Acad. Sci. U.S.A. 97*, 14091−14096.
32. Wiedenmann, J., Vallone, B., Renzi, F., Nienhaus, K., Ivanchenko, S., Röcker, C., and Nienhaus, G. U. (2005) Red fluorescent protein eqFP611 and its genetically engineered dimeric variants, *J. Biomed. Opt. 10*, 14003 (7 pages).
33. Ormö, M., Cubitt, A. B., Kallio, K., Gross, L. A., Tsien, R. Y., and Remington, S. J. (1996) Crystal structure of the Aequorea victoria green fluorescent protein, *Science 273*, 1392−1395.
34. Yang, F., Moss, L. G., and Phillips, G. N., Jr. (1996) The molecular structure of green fluorescent protein, *Nat. Biotechnol. 14*, 1246−1251.
35. Wood, T. I., Barondeau, D. P., Hitomi, C., Kassmann, C. J., Tainer, J. A., and Getzoff, E. D. (2005) Defining the role of arginine 96 in green fluorescent protein fluorophore biosynthesis, *Biochemistry 44*, 16211−16220.
36. Sniegowski, J. A., Lappe, J. W., Patel, H. N., Huffman, H. A., and Wachter, R. M. (2005) Base catalysis of chromophore formation in Arg96 and Glu222 variants of green fluorescent protein, *J. Biol. Chem. 280*, 26248−26255.
37. Reid, B. G., and Flynn, G. C. (1997) Chromophore formation in green fluorescent protein, *Biochemistry 36*, 6786−6791.
38. Heim, R., Prasher, D. C., and Tsien, R. Y. (1994) Wavelength mutations and posttranslational autoxidation of green fluorescent protein, *Proc. Natl. Acad. Sci. U.S.A. 91*, 12501−12504.
39. Barondeau, D. P., Kassmann, C. J., Tainer, J. A., and Getzoff, E. D. (2005) Understanding GFP chromophore biosynthesis: controlling backbone cyclization and modifying post-translational chemistry, *Biochemistry 44*, 1960−1970.
40. Barondeau, D. P., Putnam, C. D., Kassmann, C. J., Tainer, J. A., and Getzoff, E. D. (2003) Mechanism and energetics of green fluorescent protein chromophore synthesis revealed by trapped intermediate structures, *Proc. Natl. Acad. Sci. U.S.A. 100*, 12111−6.
41. Rosenow, M. A., Huffman, H. A., Phail, M. E., and Wachter, R. M. (2004) The crystal structure of the Y66L variant of green fluorescent protein supports a cyclization-oxidation-dehydration mechanism for chromophore maturation, *Biochemistry 43*, 4464−4472.
42. Remington, S. J., Wachter, R. M., Yarbrough, D. K., Branchaud, B., Anderson, D. C., Kallio, K., and Lukyanov, K. A. (2005) zFP538, a yellow-fluorescent protein from Zoanthus, contains a novel three-ring chromophore, *Biochemistry 44*, 202−212.
43. Gross, L. A., Baird, G. S., Hoffman, R. C., Baldridge, K. K., and Tsien, R. Y. (2000) The structure of the chromophore within DsRed, a red fluorescent protein from coral, *Proc. Natl. Acad. Sci. U.S.A. 97*, 11990−11995.
44. Lounis, B., Deich, J., Rosell, F. I., Boxer, S. G., and Moerner, W. E. (2001) Photophysics of DsRed, a red fluorescent protein, from the ensemble to the single-molecule level, *J. Phys. Chem. B 105*, 5048−5054.
45. Ivanchenko, S., Röcker, C., Oswald, F., Wiedenmann, J., and Nienhaus, G. U. (2005) Targeted Green-to-Red Photoconversion of EosFP, a Fluorescent Marker Protein, *J. Biol. Phys. 31*, 249−259.
46. Wiedenmann, J., Ivanchenko, S., Oswald, F., and Nienhaus, G. U. (2004) Identification of GFP-like Proteins in Nonbioluminescent, Azooxanthellate Anthozoa Opens New Perspectives for Bioprospecting, *Mar. Biotechnol. (NY) 6*, 270−277.
47. Nienhaus, K., Renzi, F., Vallone, B., Wiedenmann, J., and Nienhaus, G. U. (2006) Chromophore-Protein Interactions in the Anthozoan Green Fluorescent Protein asFP499, *Biophys. J.*, published online ahead of print at DOI:10.1529/biophysj.106.087411.
48. Bailey, S. (1994) The CCP4 suite: programs for protein crystallography, *Acta Crystallogr. D 50*, 760−763.
49. QUANTA software. School of Crystallography, B. C., University of London, Malet Street, London WC1E 7HX, U.K.
50. Emsley, P., and Kowtan, K. (2004) COOT Version 0.026 Model Building and Molecular Graphics System, *Acta Crystallogr. D 70*, 2126−2132.
51. PyMOL version 0.97 Molecular Graphics System. DeLano Scientific LLC.
52. Humphrey, W. F., Dalke, A., and Schulten, K. (1996) VMD−Visual Molecular Dynamics, *J. Mol. Graphics 14*, 33−38.
53. Maddalo, S. L., and Zimmer, M. (2006) The Role of the Protein Matrix in GFP Fluorescence, *Photochem. Photobiol. 82*, 367−372.
54. Pace, C. N., Vajdos, F., Fee, L., Grimsley, G., and Gray, T. (1995) How to measure and predict the molar absorption coefficient of a protein, *Protein Sci. 4*, 2411−2423.
55. Elsliger, M. A., Wachter, R. M., Hanson, G. T., Kallio, K., and Remington, S. J. (1999) Structural and spectral response of green fluorescent protein variants to changes in pH, *Biochemistry 38*, 5296−5301.
56. Chattoraj, M., King, B. A., Bublitz, G. U., and Boxer, S. G. (1996) Ultra-fast excited state dynamics in green fluorescent protein: multiple states and proton transfer, *Proc. Natl. Acad. Sci. U.S.A. 93*, 8362−8367.
57. Ward, W. W., Prentice, H. J., Roth, A. F., Cody, C. W., and Reeves, S. C. (1982) Spectral Perturbations of the *Aequorea* Green-fluorescent Protein, *Photochem. Photobiol. 35*, 803−808.
58. Lossau, H., Kummer, A., Heinecke, R., Pollinger-Dammer, F., Kompa, C., Bieser, G., Jonsson, T., Silva, C. M., Yang, M. M., Youvan, D. C., and Michel-Beyerle, M. E. (1996) Time-resolved spectroscopy of wild-type and mutant green fluorescent proteins reveals excited state deprotonation consistent with fluorophore-protein interactions, *Chem. Phys. 213*, 1−16.
59. Lill, M. A., and Helms, V. (2002) Proton shuttle in green fluorescent protein studied by dynamic simulations, *Proc. Natl. Acad. Sci. U.S.A. 99*, 2778−2781.
60. Stoner-Ma, D., Jaye, A. A., Matousek, P., Towrie, M., Meech, S. R., and Tonge, P. J. (2005) Observation of excited-state proton transfer in green fluorescent protein using ultrafast vibrational spectroscopy, *J. Am. Chem. Soc. 127*, 2864−2865.
61. Tozzini, V., and Nifosi, R. (2001) Ab Initio Molecular Dynamics of the Green Fluorescent Protein (GFP) Chromophore: An Insight into the Photoinduced Dynamics of Green Fluorescent Proteins, *J. Phys. Chem. B 105*, 5797−5803.
62. Marques, M. A., Lopez, X., Varsano, D., Castro, A., and Rubio, A. (2003) Time-dependent density-functional approach for biological chromophores: the case of the green fluorescent protein, *Phys. Rev. Lett. 90*, 258101 (4 pages).
63. Cinelli, R. A., Tozzini, V., Pellegrini, V., Beltram, F., Cerullo, G., Zavelani-Rossi, M., De Silvestri, S., Tyagi, M., and Giacca, M. (2001) Coherent dynamics of photoexcited green fluorescent proteins, *Phys. Rev. Lett. 86*, 3439−3442.
64. Hanson, G. T., McAnaney, T. B., Park, E. S., Rendell, M. E., Yarbrough, D. K., Chu, S., Xi, L., Boxer, S. G., Montrose, M. H., and Remington, S. J. (2002) Green fluorescent protein variants as ratiometric dual emission pH sensors. 1. Structural characterization and preliminary application, *Biochemistry 41*, 15477−15488.
65. Jaye, A. A., Stoner-Ma, D., Matousek, P., Towrie, M., Tonge, P. J., and Meech, S. R. (2005) Time Resolved Emission Spectra of Green Fluorescent Protein, *Photochem. Photobiol.* DOI: 10.1562/2005-05-07-RA-518.
66. Kneen, M., Farinas, J., Li, Y., and Verkman, A. S. (1998) Green fluorescent protein as a noninvasive intracellular pH indicator, *Biophys. J. 74*, 1591−1599.

67. Ward, W. W., and Bokman, S. H. (1982) Reversible denaturation of Aequorea green-fluorescent protein: physical separation and characterization of the renatured protein, *Biochemistry 21*, 4535−4540.
68. Enoki, S., Saeki, K., Maki, K., and Kuwajima, K. (2004) Acid denaturation and refolding of green fluorescent protein, *Biochemistry 43*, 14238−14248.
69. Bell, A. F., He, X., Wachter, R. M., and Tonge, P. J. (2000) Probing the ground state structure of the green fluorescent protein chromophore using Raman spectroscopy, *Biochemistry 39*, 4423−4431.
70. Niwa, H., Inouye, S., Hirano, T., Matsuno, T., Kojima, S., Kubota, M., Ohashi, M., and Tsuji, F. I. (1996) Chemical nature of the light emitter of the Aequorea green fluorescent protein, *Proc. Natl. Acad. Sci. U.S.A. 93*, 13617−13622.
71. Kummer, A. D., Kompa, C., Niwa, H., Hirano, T., Kojima, S., and Michel-Beyerle, M. E. (2002) Viscosity-dependent fluorescence decay of the GFP chromophore in solution due to fast internal conversion, *J. Phys. Chem. B 106*, 7554−7559.
72. Litvinenko, K. L., Webber, N. M., and Meech, S. R. (2001) An ultrafast polarisation spectroscopy study of internal conversion and orientational relaxation of the chromophore of the green fluorescent protein, *Chem. Phys. Lett. 346*, 47−53.
73. Litvinenko, K. L., Webber, N. M., and Meech, S. R. (2003) Internal conversion in the chromophore of the green fluorescent protein: Temperature dependence and isoviscosity analysis, *J. Phys. Chem. A 107*, 2616−2623.
74. Toniolo, A., Olsen, S., Manohar, L., and Martinez, T. J. (2004) Conical intersection dynamics in solution: the chromophore of Green Fluorescent Protein, *Faraday Discuss. 127*, 149−163.
75. Vengris, M., van Stokkum, I. H. M., He, X., Bell, A. F., Tonge, P. J., van Grondelle, R., and Larsen, D. S. (2004) Ultrafast excited and ground-state dynamics of the green fluorescent protein chromophore in solution, *J. Phys. Chem. A 108*, 4587−4598.
76. Creemers, T. M. H., Lock, A. J., Subramaniam, V., Jovin, T. M., and Völker, S. (1999) Three photoconvertible forms of green fluorescent protein identified by spectral hole-burning, *Nat. Struct. Biol. 6*, 557−560.
77. He, X., Bell, A. F., and Tonge, P. J. (2002) Isotopic Labeling and Normal-Mode Analysis of a Model Green Fluorescent Protein Chromophore, *J. Phys. Chem. B 106*, 6056−6066.
78. Esposito, A. P., Schellenberg, P., Parson, W. W., and Reid, P. J. (2001) Vibrational spectroscopy and mode assignments for an analog of the green fluorescent protein chromophore, *J. Mol. Struct. 569*, 25−41.

BI060885C